Korean J. Chem. Eng., 34(7), 1930-1935 (2017)
DOI: 10.1007/s11814-017-0057-6

pISSN: 0256-1115
eISSN: 1975-7220

A simple route for preparing Au/mesoporous silica yolk/shell particles for Au-catalyzed reactions

Young-Geon Song‡, Hochan Chang‡, and Kangtaek Lee†

Department of Chemical and Biomolecular Engineering, Yonsei University, Seoul 03722, Korea
(*Received 17 January 2017 • accepted 27 March 2017*)

Abstract−We present a simple route to prepare mesoporous hollow silica particles containing an Au core, i.e., yolk/shell particles, by sol-gel and selective etching processes. Using tetraethoxysilane as a silica precursor, zinc acetate as a base catalyst, and cetyltrimethylammonium chloride as a soft template in the presence of Au nanoparticles, double-layered mesoporous shells were produced in one step. Elemental analysis showed that the inner shell consists of zinc silicate and the outer shell is pure silica. Au/mesoporous silica yolk/shell nanoparticles were obtained by selective etching of the zinc oxide phase with citrate buffer. The particle structure and composition were studied by transmission electron microscopy with energy disperse spectroscopy, UV-vis spectroscopy, X-ray diffraction, and nitrogen sorption experiments. Formation of double shells on the Au core in a single step was explained by a difference in the formation rates of the silica and zinc silicate phases. Au/mesoporous yolk/shell particles showed a high catalytic activity for reduction of 4-nitrophenol.

Keywords: Yolk-shell, Gold, Mesoporous Silica, Mixed Oxide, Catalyst

INTRODUCTION

Noble metal nanoparticles (NPs) have attracted considerable attention for their unusual physicochemical characteristics such as catalytic property [1], localized surface plasmon resonance (LSPR) [2,3], and photoluminescence (PL) [4]. These characteristics mainly result from the large surface-to-volume ratio of NPs, which becomes significant when the size of the particles is on the nanometer scale. However, metal NPs tend to aggregate easily to form large clusters during processing, which can deteriorate their useful properties. During catalytic applications, for example, aggregation of metal NPs results in a loss of catalytic activity [5]. Therefore, protecting NPs from external conditions that can cause aggregation (e.g., pH, temperature, ionic strength, and solvent polarity) is crucial for maintaining their properties. A widely used protective method is to incorporate NPs inside the metal oxide matrix, providing high thermal stability, metal-metal oxide interaction, and ease of surface modification [6,7], Metal/mesoporous silica core/shell-type materials as catalysts have been reported to exhibit high catalytic performance with high thermal stability [8].

Although a core/shell structure is useful in protecting nanocatalysts from the external environment by preventing exposure to bulk solution and aggregation, it still has some drawbacks. For example, the surface of nanocatalysts, which provides catalytic sites, cannot be fully utilized in a core/shell structure because the shell can act as a diffusion barrier for reactants and products [8]. To overcome the drawbacks of a core/shell structure and improve catalytic activity, researchers have recently suggested novel structures such as a yolk/shell structure, which contains metal NPs inside a hollow sphere [9]. This structure not only provides a homogeneous environment around the catalytic metal surface [10], but also prevents aggregation between the metal cores [9]. Moreover, in a yolk/shell structure with a mesoporous shell, reactants in the bulk can easily diffuse into the core NPs owing to the mesoporous structure [8]. Therefore, the metal yolk/mesoporous shell structure is a promising candidate for nanocatalytic reactors with high conversion.

To date, Au/metal oxide yolk/shell structure NPs have been achieved by etching Au cores, synthesizing cores inside hollow shells [11,12], or etching the inner shell of a double layer shell [13]. During the etching of Au cores, however, a nonisotropic etching rate makes it difficult to achieve the desired morphology and size distribution of Au cores. In addition, other methods require multiple steps for fabricating a double shell structure. Recently, our group reported a simple method for preparing hollow mesoporous silica particles, in which the core/shell structure was obtained in a single step [14]. In this study, we extended this method to a simple preparation of yolk/shell-type particles containing Au cores. In this method, a mesoporous double shell around the Au core is formed in a single step, followed by etching of the inner shell. Using various experimental techniques, we characterized the structure of the yolk/shell particles, and present a mechanism for the formation of yolk/shell structures. Finally, we demonstrate the catalytic properties of the yolk/shell particles in a reduction reaction of 4-nitrophenol.

EXPERIMENTAL

1. Materials

Hydrogen tetrachloroaurate ($HAuCl_4$, 99.9%), trisodium citrate dehydrate (99%), tetraethoxysilane (TEOS, 99%), zinc acetate (Zn

†To whom correspondence should be addressed.
E-mail: ktlee@yonsei.ac.kr
‡These authors contribute this work equally.
‡This article is dedicated to Prof. Ki-Pung Yoo on the occasion of his retirement from Sogang University.

$(OAc)_2$), polyvinylpyrrolidone (PVP, MW=10,000), cetyltrimethylammonium chloride (CTAC, 25 wt% in H_2O), sodium borohydride ($NaBH_4$), and 4-nitrophenol were purchased from Sigma-Aldrich. Deionized (DI, 18 MΩ·cm) water was obtained using a Millipore water purification system. All the chemicals were used without further purification.

2. Synthesis of Yolk/Shell Nanoparticles

AuNPs with a diameter of ~15 nm were synthesized using the citrate reduction method [15]. Briefly, $HAuCl_4$ (10 mg) was dissolved in H_2O (96 mL) and the solution was heated to boiling. Then, sodium citrate solution (4 mL, 1 wt%) was added, and the mixture was allowed to react for 15 min, which produced AuNPs. The resulting AuNP suspension was cooled to room temperature and stirred for 2 h. To stabilize the AuNPs, PVP (250 mg) was added to the AuNP suspension (100 mL), followed by stirring overnight. The PVP-stabilized AuNPs were collected by centrifugation at 12,000 rpm for 30 min and redispersed in DI water (50 mL). Then, the PVP-stabilized AuNP suspension (15 mL) was mixed with CTAC (1.7 mL) and $Zn(OAc)_2$ in DI water (1 mL, 100 mg mL^{-1}) under magnetic stirring, followed by heating. When the temperature of the mixture reached 80 °C, TEOS (100 μL) was injected into the suspension to initiate the formation of a zinc silicate shell on the AuNPs. After reacting for 6 h, the suspension was cooled to room temperature, washed by repeated cycles of centrifugation and redispersion in ethanol, and calcined at 600 °C for 10 h. To obtain the yolk/shell structure, the zinc oxide phase was dissolved by adding citrate buffer (10 mL, pH 4) to the purified suspension (10 mL), followed by washing with centrifugation.

3. Reduction Reaction of 4-Nitrophenol

To investigate the catalytic property of the yolk/shell nanoparticles, 4-nitrophenol (0.025 mL, 0.005 M) in DI water was added to a mixture containing $NaBH_4$ (0.25 mL, 0.2 M) in DI water and 1.1 mL additional water. To initiate the reduction of 4-nitrophenol, the yolk/shell nanoparticle suspension (0.2 mL, 0.025 wt%) was added to the above solution. The progress of the reduction reaction was monitored by UV-vis absorption spectroscopy every 3 min.

4. Characterization

Transmission electron microscopy with energy dispersive X-ray analysis (TEM-EDX, JEOL JEM-2010 and JEM-2100, 200 kV) was used to observe the morphology of the synthesized particles and to determine their composition. X-ray diffraction (XRD, Rigaku Smartlab diffractometer), with an excitation power of 9 kW (45 kV, 200 mA), was used to confirm the structure of the particles. Nitrogen sorption experiment at 77 K was conducted using a Micromeritics ASAP 2020 system to investigate the pore structure and properties of the particles. UV-vis absorption spectroscopy (Shimadzu 1650 PC spectrophotometer) was used to observe the surface plasmon resonance band of AuNPs and to monitor the reduction reaction of 4-nitrophenol.

RESULTS AND DISCUSSION

Au/mesoporous silica (m-SiO_2) yolk/shell particles were prepared as follows. We synthesized spherical AuNPs using the typical citrate reduction method. The synthesized AuNPs were then functionalized with PVP for steric stabilization, and then, purified by centrifugation or dialysis. To grow the mesoporous shell on the surface of AuNPs, TEOS, CTAC, and Zn $(OAc)_2$ were added to the suspension of the PVP-stabilized AuNPs, followed by a sol-gel reaction at 80 °C for 6 h. Subsequently, CTAC molecules were removed by calcination to generate mesopores in the shell. This reaction, which is similar to our previous work on the synthesis of mesoporous zinc silicate particles [14], produced particles with a core/shell structure (Fig. 1(a)) in which the diameter of the Au core and

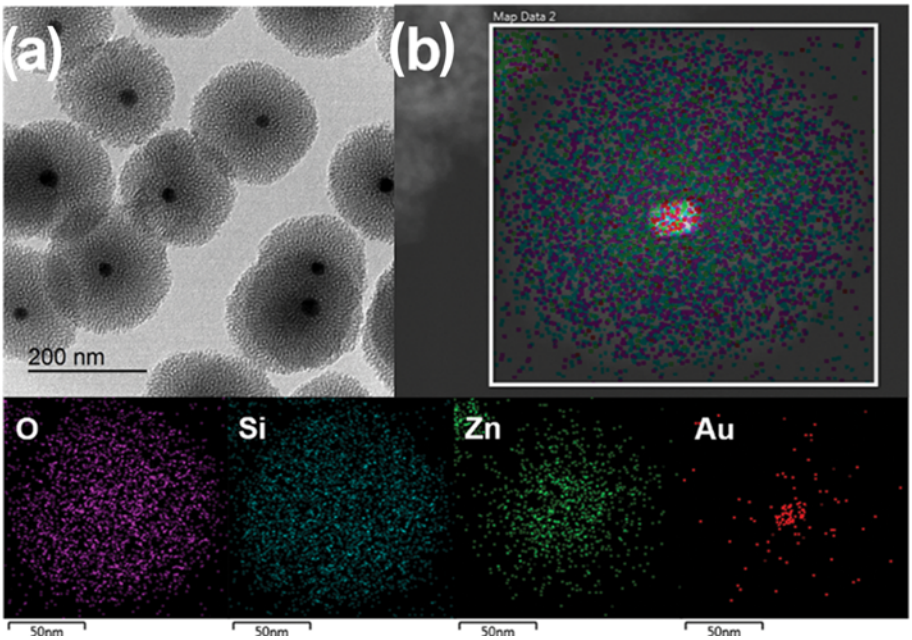

Fig. 1. TEM image of calcined Au/mesoporous zinc silicate core/shell nanoparticles (a) and EDX elemental mapping of particles (b) before etching ZnO.

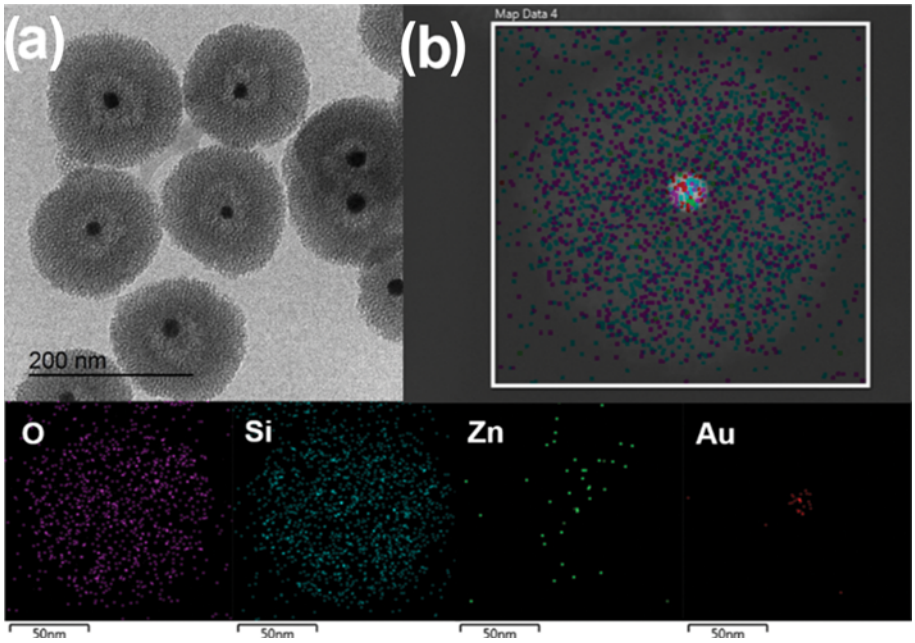

Fig. 2. TEM image of calcined Au/hollow mesoporous SiO_2 particles (a) and EDX elemental mapping of particles (b) after etching ZnO.

the overall shell thickness was ~13.0 nm and ~85.7 nm, respectively. In addition, a distinct boundary was present in the mesoporous shell, exhibiting a double shell structure with an inner (darker) shell (~58.9 nm thick) and an outer (lighter) shell (~26.8 nm thick). Purification of the PVP-stabilized AuNPs by either centrifugation or dialysis was crucial for uniform shell growth. To determine the composition of the core/double-shell particles, we performed elemental analysis. The energy dispersive X-ray analysis (EDX) results in Fig. 1(b) show that Zn was present predominantly in the inner shell, whereas Si and O were present in both the inner and outer shells, indicating that the inner shell consists of a mixed oxide (ZnO-SiO_2), whereas the outer shell consists of SiO_2, which is consistent with the mesoporous zinc silicate particles [14].

Next, the ZnO phase in the inner shell was selectively etched out by addition of citrate buffer at pH 4 [16]. Fig. 2(a) shows the resultant particles with the yolk/shell structure where the inner shell appears hollow. EDX results confirm that most of the Zn species disappeared during the etching step (Fig. 2(b)), suggesting that the ZnO phase in the inner shell of the core/double-shell structure was selectively etched by the citrate buffer. We also suspect that residual Zn species after etching step mainly comes from a background noise. Therefore, it is reasonable to expect that Zn concentration is extremely low in the yolk/shell particles so its effect can be ignored. Fig. 3 shows that most of the Au cores are located at the center of the particles, which indicates that Au cores are immobile because they are held by the SiO_2 network inside the inner shell.

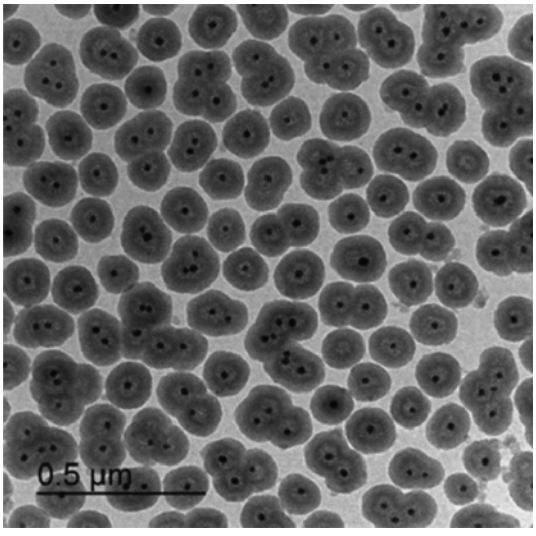

Fig. 3. TEM image of Au/hollow mesoporous SiO_2 particles at low magnification.

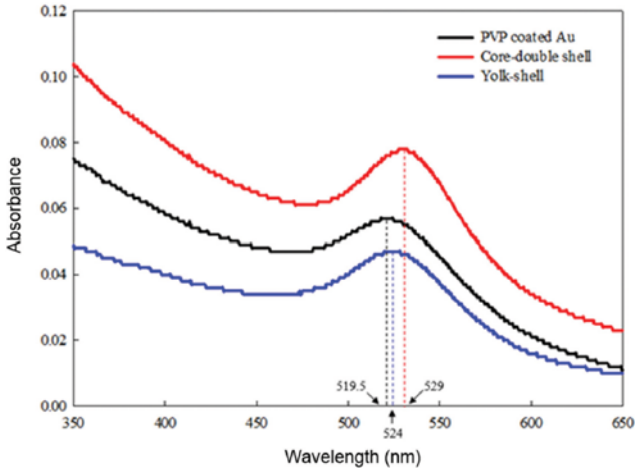

Fig. 4. UV absorption spectra of PVP-coated AuNPs, Au/zinc silicate core/shell particles, and Au/hollow m-SiO_2 particles.

Fig. 4 compares the UV-vis absorption spectra of the synthesized particles. The PVP-stabilized AuNPs initially showed a surface plasmon resonance peak at 519.5 nm in ethanol, whose refractive index n is 1.36. When the surface of the AuNPs was coated with a zinc silicate double shell, the surface plasmon resonance band red-shifted to 529 nm because ZnO around an Au core has a higher refractive index (n=2.003) than ethanol. However, etching the ZnO phases from the inner shell blue-shifted the surface plasmon band to 524 nm because the refractive index of SiO_2 (n=1.458) is lower than that of ZnO. Therefore, predictions from the Mie theory confirm that most of the ZnO phase was dissolved during the etching process. Furthermore, the fact that etching did not blue-shift the surface plasmon band to 519.5 nm (i.e., AuNPs) suggests that the local refractive index of the surrounding medium around an Au core is still higher than that of pure ethanol [17].

To investigate the structure of the yolk/shell particles further, we performed XRD and nitrogen sorption experiments. Fig. 5(a) shows four diffraction peaks for the yolk/shell particles at 2θ=38.22°, 44.43°, 64.62°, and 76.58°, corresponding to the (111), (200), (220), and (311) lattice planes of bulk gold, and the peak in the range of 2θ=17-30° reveals typical diffraction patterns of amorphous silica. The small angle XRD pattern also shows a single peak (2θ=0.78°) below 2θ=10°, revealing disordered mesoporous silica structure [18,19]. Fig. 5(b) shows typical type IV isotherms, indicating a mesoporous structure in the shell. The adsorption and desorption isotherms display two hysteresis loops of yolk/shell particles at a relative pressure (P/P_0) higher than 0.45 and at P/P_0>0.9, which are related to the mesopores inside the yolk/shell particles and the interparticle porosities, respectively. Using the Barrett-Joyner-Halenda (BJH) method, the specific surface area and the average pore diameter of the yolk/shell particles were calculated to be 194.42 $m^2 g^{-1}$ and 3.83 nm, respectively.

The formation mechanism of the yolk/shell particles can be explained as follows. It is well known that CTAC molecules form micelles in aqueous solution above the critical micelle concentration, acting as a soft template for the mesoporous structure [20]. In our previous work, we showed that $Zn(OAc)_2$ not only catalyzes the hydrolysis reaction of TEOS, but is also hydrolyzed to form a mixed oxide ($ZnO\text{-}SiO_2$). Since the formation rate of the mixed oxide is much faster than that of pure silica [14], positively charged CTAC micelles are coated with a negatively charged mixed oxide phase. These micelles then aggregate on the Au surface to form a mesoporous $ZnO\text{-}SiO_2$ inner shell. Here, the formation of zinc-silicate particles in the absence of Au cores is unfavorable because AuNPs act as a seed. After depletion of Zn^{2+} ions, CTAC micelles are coated with SiO_2, and they aggregate on the growing particles, forming a mesoporous SiO_2 outer shell. Therefore, formation of a double shell via a one-step process results from a difference in the formation rates of silica and mixed oxide, as reported previously [14]. When the AuNPs were not stabilized by PVP or thoroughly washed, however, aggregation of AuNPs or uncontrolled shell growth occurred. Finally, the ZnO phases were dissolved by citrate buffer at pH 4 to yield the yolk/shell structure. This mechanism is summarized in Fig. 6.

To explore the possibility of using yolk/shell NPs as catalysts, we investigated the reduction reaction of 4-nitrophenol. With an Au catalyst, 4-nitrophenol is reduced to 4-aminophenol, changing the color of the solution from bright yellow to colorless [21]. Progress of this reaction can be easily monitored by UV-vis absorption spectroscopy. After addition of the yolk/shell particles, the absorbance of 4-nitrophenol at 400 nm gradually decreased with time, while the absorbance of 4-aminophenol at 295 nm increased (Fig. 7). These results demonstrate that yolk/shell particles act as a catalyst in the reduction of 4-nitrophenol. From relative absorbance at time t and zero (A_t and A_0, respectively), we could calculate $\ln(C_t/C_0)$, where C_t and C_0 represent the concentrations of 4-nitrophenol at times t and zero, respectively. The inset of Fig. 7 shows that a plot of $\ln(C_t/C_0)$ vs. reaction time is linear, indicating that the reduction of 4-nitrophenol is a pseudo-first-order reaction. From the slope, the rate constant of the reduction reaction was estimated to be 0.0016 s^{-1}. Although there are SiO_2 networks between the Au cores and the mesoporous silica outer shell, the reduction rate is analogous to previous results with similar core sizes [8]. Therefore, we concluded that the synthesized yolk/shell particles can be

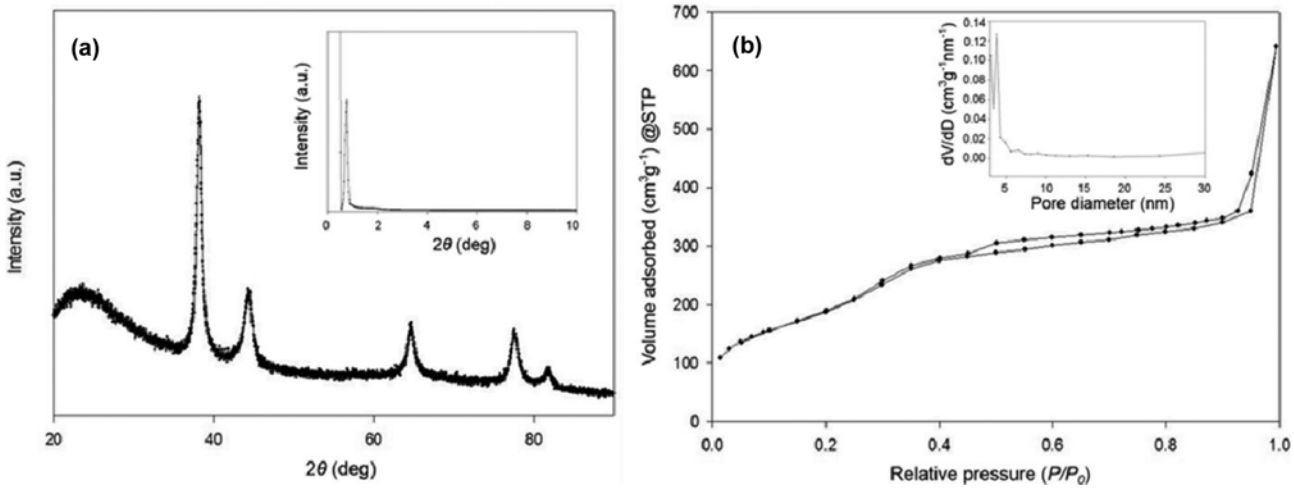

Fig. 5. (a) XRD pattern (inset is small angle XRD pattern) and (b) nitrogen adsorption-desorption isotherms (the inset shows BJH pore size distribution) of the Au/m-SiO_2 yolk/shell particles.

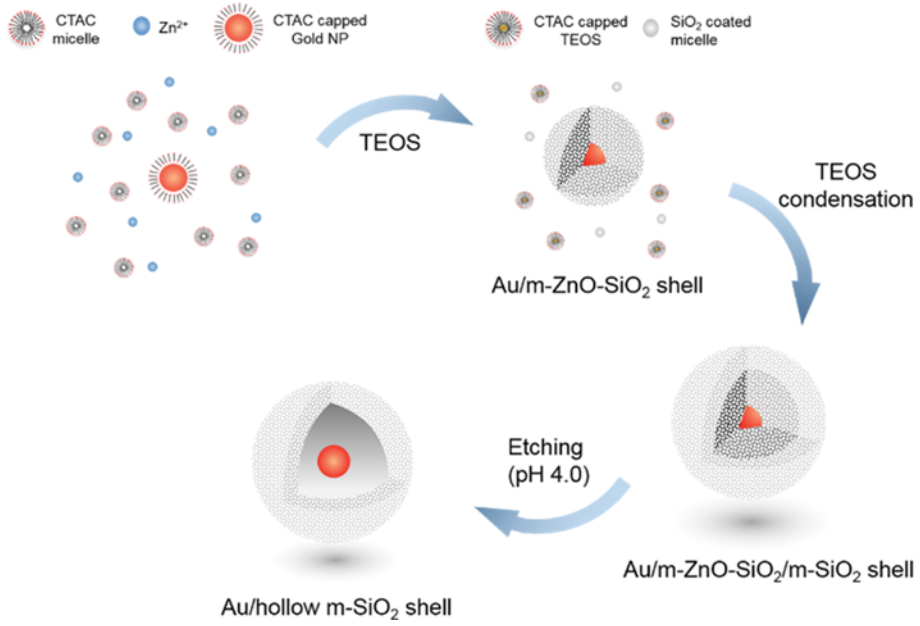

Fig. 6. Schematic illustration of preparation for Au/m-SiO_2 yolk/shell particles.

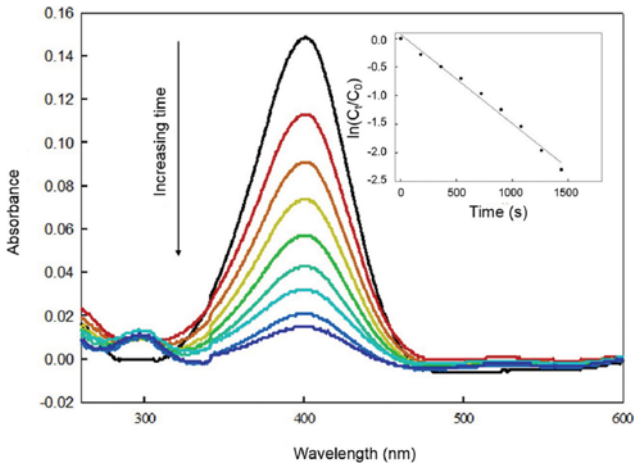

Fig. 7. Time-dependent UV-vis spectra of a reduction reaction in the presence of Au/m-SiO_2 yolk/shell particles and plot of $\ln(C_t/C_0)$ as a function of the reaction time (inset).

used as catalysts for the reduction of 4-nitrophenol.

CONCLUSIONS

Since manipulation of the nanocatalyst structure can enhance catalytic activity and stability, we have developed a novel route for preparing Au/m-SiO_2 yolk/shell particles for catalytic applications. Using this route, a double-layered shell could be formed on the AuNP surface in a single reaction step. By dissolving the zinc oxide phase present in the inner shell, we obtained Au/m-SiO_2 yolk/shell particles. This strategy provides a simple, fast, and easy route for preparing yolk/shell structures under mild conditions, compared to the conventional methods. The as-prepared Au/m-SiO_2 yolk/shell particles exhibited a high catalytic ability in the reduction reaction of 4-nitrophenol. We believe that this method will be useful in the design of catalysts, nanoreactors, and nanocarriers.

ACKNOWLEDGEMENT

This work was supported by a grant from the National Research Foundation of Korea (No. 2014R1A2A1A11051436).

REFERENCES

1. S. Peng, Y. Lee, C. Wang, H. Yin, S. Dai and S. Sun, *Nano Res.*, **1**, 229 (2008).
2. M. Chen, H. H. Cai, F. Yang, D. Lin, P. H. Yang and J. Cai, *Spectrochim. Acta, Part A*, **118**, 776 (2014).
3. D. X. Li, J. F. Zhang, Y. H. Jang, Y. J. Jang, D. H. Kim and J. S. Kim, *Small*, **8**, 1442 (2012).
4. M. Cui, Y. Zhao and Q. Song, *TrAC, Trends Anal. Chem.*, **57**, 73 (2014).
5. S.-J. Park, J. W. Bae, G.-I. Jung, K.-S. Ha, K.-W. Jun, Y.-J. Lee and H.-G. Park, *Appl. Catal., A*, **413-414**, 310 (2012).
6. C. Chen, C. Nan, D. Wang, Q. Su, H. Duan, X. Liu, L. Zhang, D. Chu, W. Song, Q. Peng and Y. Li, *Angew. Chem., Int. Ed. Engl.*, **50**, 3725 (2011).
7. C. Y. Ma, Z. Mu, J. J. Li, Y. G. Jin, J. Cheng, G. Q. Lu, Z. P. Hao and S. Z. Qiao, *J. Am. Chem. Soc.*, **132**, 2608 (2010).
8. J. Chen, R. Zhang, L. Han, B. Tu and D. Zhao, *Nano Res.*, **6**, 871 (2013).
9. G. Li and Z. Tang, *Nanoscale*, **6**, 3995 (2014).
10. J. C. Park and H. Song, *Nano Res.*, **4**, 33 (2010).
11. J. Lee, J. C. Park, J. U. Bang and H. Song, *Chem. Mater.*, **20**, 5839 (2008).
12. J. Lee, J. C. Park and H. Song, *Adv. Mater.*, **20**, 1523 (2008).
13. S. Wang, M. Zhang and W. Zhang, *ACS Catal.*, **1**, 207 (2011).

14. H. Choi, K. Um, M. Im and K. Lee, *Chem. Mater.*, **27**, 2343 (2015).
15. J. Turkevich, P. C. Stevenson and J. Hillier, *Discuss. Faraday Soc.*, **11**, 55 (1951).
16. J. Zhai, X. Tao, Y. Pu, X.-F. Zeng and J.-F. Chen, *Appl. Surf. Sci.*, **257**, 393 (2010).
17. L. M. Liz-Marzan, M. Giersig and P. Mulvaney, *Langmuir*, **12**, 4329 (1996).
18. J. S. Beck, J. C. Vartuli, W. J. Roth, M. E. Leonowicz, C. T. Kresge, K. D. Schmitt, C. T. W. Chu, D. H. Olson, E. W. Sheppard, S. B. Mccullen, J. B. Higgins and J. L. Schlenker, *J. Am. Chem. Soc.*, **114**, 10834 (1992).
19. Y. Ishii, Y. Nishiwaki, A. Al-zubaidi and S. Kawasaki, *J. Phys. Chem. C*, **117**, 18120 (2013).
20. M. P. Pileni, *Nat. Mater.*, **2**, 145 (2003).
21. S. Wunder, F. Polzer, Y. Lu, Y. Mei and M. Ballauff, *J. Phys. Chem. C*, **114**, 8814 (2010).